Research article

Journal of Applied Toxicology

Received: 5 February 2016, Revised: 19 February 2016, Accepted: 22 February 2016 Published online in Wiley Online Library: 22 April 2016

(wileyonlinelibrary.com) DOI 10.1002/jat.3323

Biodistribution of polyacrylic acid-coated iron oxide nanoparticles is associated with proinflammatory activation and liver toxicity

Diana Couto[a], Marisa Freitas[a], Vera Marisa Costa[b], Renan Campos Chisté[a], Agostinho Almeida[c], M. Arturo Lopez-Quintela[d], José Rivas[e], Paulo Freitas[e], Paula Silva[f], Félix Carvalho[b]* and Eduarda Fernandes[a]*

ABSTRACT: Iron oxide nanoparticles (IONs) have physical and chemical properties that render them useful for several new biomedical applications. Still, so far, *in vivo* safety studies of IONs with coatings of biomedical interest are still scarce. The aim of this study, therefore, was to clarify the acute biological effects of polyacrylic acid (PAA)-coated IONs, by determining their biodistribution and their potential proinflammatory and toxic effects in CD-1 mice. The biodistribution of PAA-coated IONs in several organs (liver, spleen, kidneys, brain, heart, testes and lungs), the plasma cytokines, chemokine and aminotransferases levels, white blood cell count, oxidative stress parameters, adenosine triphosphate and histologic features of liver, spleen and kidneys were evaluated 24 h after a single acute (8, 20 or 50 mg kg^{-1}) intravenous administration of PAA-coated IONs in magnetite form. The obtained results showed that these IONs accumulate mainly in the liver and spleen and, to a lesser extent, in the lungs. Although our data showed that PAA-coated IONs do not cause severe organ damage, an inflammatory process was triggered *in vivo*, as evidenced by as evidenced by increased neutrophils and large lymphocytes in the differential blood count. Moreover, an accumulation of iron in macrophages of the liver and spleen was observed and hepatic lipid peroxidation was elicited, showing that the IONs are able to induce oxidative stress. The effects of these nanoparticles need to be further investigated regarding the mechanisms involved and the long-term consequences of intravenous administration of PAA-coated IONs. Copyright © 2016 John Wiley & Sons, Ltd.

Keywords: iron oxide nanoparticles; biodistribution; inflammation; lipid peroxidation; bioaccumulation

Introduction

The use of nanoparticles (NPs) is considered a promising strategy in the development of new biomedical applications, due to their distinctive physical and chemical properties (Weinstein *et al.,* 2010). Among the different types of NPs used for biomedical applications, iron oxide NPs (IONs) are one of the most common (Shubayev *et al.,* 2009). Several formulations of these NPs are used mainly for magnetic resonance imaging and diagnosis (Farrell *et al.,* 2013; Weinstein *et al.,* 2010) and they are presently being investigated for cancer treatment with the concurrent use of hyperthermia (Maier-Hauff *et al.,* 2007, 2011), and in inflammation imaging (Alkins *et al.,* 2013; Farrell *et al.,* 2013; Weinstein *et al.,* 2010). The human exposure to IONs is usually acute in resonance imaging, this procedure being often repeated throughout the patients' life (Corot *et al.,* 2006; Ross *et al.,* 2009).

So far, the IONs available in the market are always coated, as coating is regarded as an improvement on their biocompatibility. The most common coatings are based on dextran and its derivatives (Corot *et al.,* 2006), though other coatings are presently being tested. Recently, polyacrylic acid (PAA), an aqueous soluble polymer, has been shown to be a promising coating agent in gene delivery (Cao *et al.,* 2013).

Despite the widespread use of IONs, safety issues are still a matter of debate. In fact, *in vitro* studies using different cellular models have reported that IONs regardless of their coating may cause increased production of reactive oxygen species (ROS), activation of inflammatory pathways and cell death, among other adverse effects (Ahamed *et al.,* 2013). In our previous *in vitro* studies, we have demonstrated that PAA-coated IONs in magnetite form are

* *Correspondence to: Eduarda Fernandes, PharmD, PhD, UCIBIO-REQUIMTE, Laboratory of Applied Chemistry, Department of Chemical Sciences, Faculty of Pharmacy, University of Porto, Porto, Portugal, Rua de Jorge Viterbo Ferreira n° 228, 4050-313 Porto, Portugal.*
E-mail: egracas@ff.up.pt

Félix Carvalho, PharmD, PhD, UCIBIO-REQUIMTE, Laboratory of Toxicology, Department of Biological Sciences, Faculty of Pharmacy, University of Porto, Porto, Portugal, Rua de Jorge Viterbo Ferreira no. 228, 4050-313 Porto, Portugal.
E-mail: felixdc@ff.up.pt

[a]*UCIBIO-REQUIMTE, Laboratory of Applied Chemistry, Department of Chemical Sciences, Faculty of Pharmacy, University of Porto, Porto, Portugal*

[b]*UCIBIO-REQUIMTE, Laboratory of Toxicology, Department of Biological Sciences, Faculty of Pharmacy, University of Porto, Porto, Portugal*

[c]*LAQV-REQUIMTE, Laboratory of Applied Chemistry, Department of Chemical Sciences, Faculty of Pharmacy, University of Porto, Porto, Portugal*

[d]*Laboratory of Nanotechnology and Magnetism, Institute of Technological Research, IIT, University of Santiago de Compostela (USC), Spain*

[e]*International Iberian Nanotechnology Laboratory, Braga, Portugal*

[f]*UCIBIO-REQUIMTE, Laboratory of Histology and Embryology, Institute of Biomedical Sciences Abel Salazar (ICBAS), University of Porto, Porto, Portugal*

able to trigger the production of ROS in human neutrophils, eliciting apoptosis in that cellular model (Couto *et al.,* 2014). We have also found that the same PAA-coated IONs have the ability to induce cytokine (interleukin [IL]-6, IL-8, IL-10, tumor necrosis factor [TNF]-α, interferon [IFN]-γ, and IL-1β via transforming growth factor beta activated kinase production and p38 mitogen-activated protein kinase) activation in human blood cells (Couto *et al.,* 2015). Altogether, these results show that PAA-coated IONs have a proinflammatory potential that needs further investigation.

There are few *in vivo* studies performed so far to evaluate the potential toxic effects of IONs. In mice, Fe_3O_4 NPs triggered hepatic and renal damage (Ma *et al.,* 2012), whereas in humans the administration of IONs in magnetic resonance imaging caused some adverse effects, namely urticaria (Anzai *et al.,* 2003; Hudgins *et al.,* 2002; Keller *et al.,* 2004; Ross *et al.,* 2009), diarrhea (Anzai *et al.,* 2003), some allergic reactions (Ross *et al.,* 2009), nausea (Anzai *et al.,* 2003; Mack *et al.,* 2002), headaches (Anzai *et al.,* 2003; Hudgins *et al.,* 2002), back and chest pain (Anzai *et al.,* 2003; Keller *et al.,* 2004), flush (Keller *et al.,* 2004), dyspnea (Keller *et al.,* 2004), vertigo (Mack *et al.,* 2002), erythema (Keller *et al.,* 2004), skin discoloration (McCauley *et al.,* 2002), pruritus (Hudgins *et al.,* 2002; Keller *et al.,* 2004) and vasodilatation (Anzai *et al.,* 2003). Regarding PAA-coated IONs, to the best of our knowledge, there is only one *in vivo* study that evaluated, in mice, the basic functions of the renal and cardiovascular systems, 24 h and 96 h after a 10 mg kg^{-1} intravenous (i.v.) injection of PAA-coated γ-IONs (Iversen *et al.,* 2013). The results obtained by Iversen *et al.* (2013) suggest that these IONs do not affect kidney function but decrease blood pressure temporarily.

The aim of this work was to clarify the effects of single acute PAA-coated IONs i.v. administration, by determining their biodistribution in several organs (liver, spleen, kidneys, brain, heart, testes and lungs) and the potential proinflammatory and toxic effects in CD-1 mice. Histological analyses of liver, spleen and kidneys were done and oxidative stress and energetic status on liver and kidneys were performed.

Materials and methods

Chemicals

Isoflurane (Isoflo®) was obtained from Abbott Animal Health (Illinois, USA). Iron standard for atomic absorption spectrometry (Trace CERT®; 1000 mg l^{-1}) and concentrated nitric acid (*Trace*SELECT®; ≥69.0% w/w) were obtained from Fluka (L'Isle d'Abeau Chesnes, France) and hydrogen peroxide solution (*Trace*SELECT® Ultra; ≥30% v/v) from Fluka (Seelze, Germany). Ultrapure water (resistivity >18.2 MΩ.cm at 25 °C) was obtained from a Sartorius (Sartorius, Germany) arium®pro water purification system. Sodium hydroxide, potassium bicarbonate and Histosec® pastilles (paraffin) were acquired from Merck (Darmstadt, Germany). Ethanol was obtained from Panreac AppliChem (Darmstadt, Germany). BD™ Cytometric Bead Array was acquired from BD Biosciences (San Diego, USA). RC DC Protein Assay kit was obtained from Bio-Rad (St Louis, USA). ABX Pentra reagents were purchased from HORIBA (Kyoto, Japan). Commercial 4% buffered formalin was purchased from Klinipath (VB Duiven,the Netherlands). Xylene (BDH Prolabo) was obtained from VWR International (Dublin, Ireland). All other reagents were obtained from Sigma Chemical Co. (St Louis, USA), from the highest purity available.

Characterization of the polyacrylic acid-coated iron oxide nanoparticles

PAA-coated magnetite particles were obtained from Nanogap (Coruña, Spain), and their preparation and physico-chemical characterization was performed as previously reported (Couto *et al.,* 2014). Characterization was accomplished by transmission electron microscopy, using a Hitachi (Tokyo, Japan) H-7000 microscope. The determination of the hydrodynamic size and zeta potential of NPs was performed in 0.9% saline solution, using an HORIBA (Kyoto, Japan) SZ-100 NP analyzer (532 nm DPSS laser). PAA-coated IONs had a mean particle size of 10.1 ± 2.4 nm (mean ± standard deviation). When the IONs were dispersed in normal saline, a large hydrodynamic size (46.7 ± 12 nm) was observed and the zeta potential was −1.56 ± 0.45 mV.

Animal treatment

Male mice (8 weeks) of CD-1 strain, from Charles River laboratories (Chatillon-sur-Chalaronne, France), weighing 30–40 g were used in this study. Upon arrival, the animals were randomly housed in cages (four animals per cage) and, after, they were maintained under a controlled environment (22.0 ± 2.0 °C, 40% relative humidity, in 12 h light/dark cycles, at the Institute for Biomedical Sciences Abel Salazar-University of Porto animal house facility). The animals had *ad libitum* access to food and water, and permanent veterinary supervision throughout the experimental period.

All efforts were made to provide appropriate animal care, minimizing their suffering. Housing and experimental treatment of the animals were in accordance with the guidelines defined by the European Council Directive (2010/63/EU) transposed into Portuguese law (Decreto-Lei number 113/2013, August 7). Moreover, the experiments were performed with the approval of the Ethical Committee of the Faculty of Pharmacy, University of Porto (opinion number July 19, 2014). Animals were left to acclimate for 10 days, before the experiments started.

Administration of polyacrylic acid-coated iron oxide nanoparticles

Administration of PAA-coated IONs was performed through an i.v. injection in the tail vein, by experienced veterinarians. All stock solutions of the NPs were prepared daily in sterile conditions and PAA-coated IONs were suspended in 0.9% saline solution. Four groups were created with six animals each: control, and animals dosed at 8, 20 or 50 mg kg^{-1}. The 0.9% saline solution was administered to control animals on the same schedule and at the same equivalent volume of PAA-coated IONs-dosed animals. Animal weight was assessed before and 24 h after the i.v. administration of the PAA-coated IONs, and animals were killed 24 h after dosing.

In humans, the use of IONs for imaging procedures has been reported at doses between 2 and 7 mg kg^{-1} (Kooi *et al.,* 2003; Qiu *et al.,* 2012). In this study, the equivalence to the doses used in humans was calculated according to the allometric scaling principles using the formula: human dose (mg kg^{-1}) = animal dose (mg kg^{-1}) × (animal weight/human weight)$^{1/4}$ (Hayes, 2001). Thus, the equivalent dose in mice (30 g) to a 7 mg kg^{-1} dose in a 70 kg man is approximately 49 mg kg^{-1}. Therefore, the present study has human relevance as human pharmacological relevant doses were used.

Blood and organ collection

Animals were anesthetized and killed with isoflurane 24 h after the PAA-coated IONs dosing. Blood was immediately collected from the inferior vena cava. A drop of blood was used for smears, whereas the remaining blood was placed into Vacutainer™ EDTA tubes (BD Biosciences). Subsequently, the blood was centrifuged at 920 *g*, for 10 min, at 4 °C, and plasma was separated and stored at −20 °C for posterior cytokine, total creatine kinase (CK), aspartate aminotransferase (AST) and alanine aminotransferase (ALT) analysis. Immediately after death, the liver, spleen, kidneys, brain, heart, testes and lungs were collected and weighed. The tail of the mouse was also collected.

For iron determination in mice organs, a small sample (with a variable weight depending on the organ, not exceeding 200 mg) of tissue and the whole tail were used. Because of possible contamination of blood, it was thoroughly washed with ultrapure water and strong agitation. The organ samples were stored in decontaminated polypropylene tubes at 4 °C until analysis.

A portion of the liver, spleen and kidney in controls and 50 mg kg^{-1} PAA-coated IONs dosed animals was taken for histological analysis, which will be described below.

The remaining liver and kidney tissue samples were homogenized in ice-cold phosphate-buffered solution 0.1 M KH_2PO_4 pH 7.4 in an homogenizer, and processed, as previously described (Dores-Sousa *et al.,* 2015). An aliquot of the homogenates was placed in cold $HClO_4$ [5% (m/v) final acid concentration], with 0.05% (m/v) of antioxidant butylated hydroxytoluene and immediately frozen at −80 °C (for a maximum of 1 month) until malondialdehyde (MDA) determination by high pressure liquid chromatography (HPLC). Another aliquot of the homogenates was treated with $HClO_4$ [5% (m/v) final acid concentration] and centrifuged at 16 000 *g* for 10 min at 4 °C. The resulting supernatant was separated and frozen at −80 °C for total glutathione (GSHt), oxidized GSH (GSSG) and adenosine triphosphate (ATP) determinations. The remaining homogenate was stored at −20 °C for protein determination.

Measurement of plasma biomarkers

CK, AST and ALT were determined using enzymatic assays in the apparatus ABX Pentra 400 with ABX Pentra reagents (HORIBA), according to the manufacturer's instructions.

Plasma cytokines and chemokine determination

Cytokines (IL-6, IL-10, IFN-γ, TNF-α, IL-12p70) and the chemokine, monocyte chemoattractant protein-1, were determined in plasma using a BD™ Cytometric Bead Array (BD Biosciences), according to the manufacturer's instructions. Fluorescence signals for each sample were collected using BD Accuri™ C6 flow cytometer (BD Biosciences) equipped with 488 nm and 640 nm lasers. Data were analyzed using FCAP Array™ software, version 3.0 (Soft Flow, USA).

Differential leukocyte counts in peripheral blood smears

Blood smears were made on glass slides and air-dried. At least two blood smears were prepared per animal. The slides were stained using the Diff-Quik procedure, and a manual differential count of 100 leukocytes was performed under oil-immersion lens. Leukocyte nomenclature and morphology have been described previously for mouse (Bolliger and Everds, 2010), and used accordingly in this study.

Iron determination in organs

Sample treatment and iron determination were performed as previously described (Ramos *et al.,* 2014). Samples were placed in a dry oven at 110 °C until they attained constant weight (dry sample weight) (approximately 24 h). Dried samples were weighed and placed in the microwave oven digestion vessels, previously decontaminated with 10% (v/v) nitric acid and thoroughly rinsed with ultrapure water. Samples were digested using 2 ml of concentrated HNO_3 and 0.5 ml of H_2O_2 (except for the tail, where 4 ml and 1 ml, respectively, were used). The sample digestion was performed in a MLS 1200 mega microwave oven from Milestone (Sorisole, Italy) equipped with an HPR 1000/10 rotor using the following power (W)/time (min) program: 250/1, 0/2, 250/5, 400/5 and 600/5. After cooling, sample solutions were made up to 25 ml with ultrapure water (50 ml for tail samples) and stored in closed propylene tubes at 4 °C until analysis. For each digestion batch (10 samples), a sample blank was also determined.

Iron determination was performed using a PerkinElmer (Überlingen, Germany) model 3100 atomic absorption spectrometer. An Intensitron™ (PerkinElmer) hollow cathode lamp was used as a light source (λ = 248.3 nm).

Calibration standards were prepared by diluting the commercial iron standard with 0.2% (v/v) HNO_3 solution. Calibration curves were obtained with five calibration standards with concentrations ranging from 0 to 4 mg l^{-1}. Data were expressed as μg of iron per g of tissue, on a dry basis.

Histological analysis

To assess the effect of PAA-coated ION administration on liver, spleen and kidneys histology, basic histopathological analysis of the animals exposed to the highest dose (50 mg kg^{-1}) was performed. In this study, liver was cut into approximately 4 mm thick slabs and then a systematic selection was carried out and sampled pieces were processed for light microscopy. The spleen was cut in two halves along the midsagittal plane. The kidneys were divided in to two equal parts: the cranial and caudal parts. Each half of both organs was then randomly selected for histological analysis. The organs were fixed in commercial 4% buffered formalin. After fixation (24 h), the tissues were dehydrated through a series of graded ethanol solutions (70–99.8%), cleared with xylene, and then impregnated and embedded in paraffin. Each organ was entirely sectioned using a Leica Biosystems (Heidelberg, Germany) RM 2125 microtome into 5 μm thick sections. For improving adhesion, the sampled sections were mounted in silane-coated microscope slides (Nuova Aptaca, Canelli, Italy). From each organ, the first section to be sampled was randomly selected. Four successive slides, with an equal number of sequential sections each, were set aside for posterior analysis. From every fifth slide a group of four slides were chosen for histological analysis. This allowed for analysis of the entire organ to check the existence of focal lesions. The sections were then stained according to the following scheme: (1) hematoxylin–eosin (H&E); (2) Perls' Prussian blue; (3) H&E; (4) Masson's trichrome (Bancroft and Gamble, 2008).

Oxidative stress parameters

Glutathione evaluation. The GSHt and GSSG levels of tissue homogenates were determined by the 5,5′-dithio-bis(2-nitrobenzoic acid-GSSG reductase recycling assay, as previously described (Dores-Sousa *et al.,* 2015). For GSSG determination, 10 μl of 2-

vinylpyridine was added to the acidic supernatant and shaken for 1 h in ice to block the thiol group in GSH. Then, the determination of GSSG was performed, as described (Dores-Sousa *et al.,* 2015). The GSH was calculated using the following formula GSH = GSHt – 2 GSSG.

GSH and GSSG standard solutions (0–15 and 0–8 μM, respectively) were prepared in 5% (m/v) $HClO_4$ and results were expressed as nmol mg^{-1} protein.

Lipid peroxidation. Lipid peroxidation was evaluated by HPLC determination of MDA (Dores-Sousa *et al.,* 2015), with some modifications. Briefly, the acidic liver and kidney homogenates were centrifuged (16 000 *g*, 5 min, at 4 °C) and 200 μl of the resulting supernatant were incubated with 200 μl of thiobarbituric acid (0.8% in water) for 60 min at 80 °C in a water bath. After cooling, 20 μl of the samples were injected into the HPLC system (LC-2000 Plus; Jasco) (Easton, USA), equipped with quaternary pumps (PU-2089 Plus), an autosampler (AS-2057 Plus) and a fluorescence detector (FP-2020 Plus). MDA was separated on a Synergi™ 4 μm Hydro-RP column (250 × 4.6mm; Phenomenex) (Torrance, USA), with a mobile phase consisting of 80 : 20 (v/v) ammonium acetate aqueous solution (10 mM, pH 6.8) and acetonitrile in an isocratic mode at a flow rate of 1.0 ml min^{-1} and at room temperature. The fluorescence detector was set at $\lambda_{excitation} = 525$ nm and $\lambda_{emission} = 560$ nm. MDA was quantified by external calibration using a seven-point analytical curve (0–3 μM). The MDA content was expressed as pmol MDA mg^{-1} protein.

Adenosine triphosphate measurement

ATP measurement in liver and kidney homogenates was performed by the luciferin/luciferase bioluminescence assay, as described before (Rossato *et al.,* 2014). Briefly, 150 μl of tissue homogenates were neutralized with 150 μl of 0.76 M $KHCO_3$ and centrifuged at 16 000 *g*, for 1 min, at 4 °C. ATP levels were quantified after the reaction of 100 μl of neutralized supernatant with the luciferin/luciferase solution. ATP standards (0–10 μM) were prepared in 5% (m/v) $HClO_4$. ATP intracellular levels were expressed as nmol mg^{-1} protein.

Protein determination

Protein content was determined with the RC DC™ Protein Assay kit (Bio-Rad), according to the manufacturer's instructions. Bovine serum albumin (0–1.2 mg ml^{-1}) was used as standard.

Statistical analysis

Results are expressed as the mean ± SEM. Statistical comparisons were made between control and PAA-coated IONs treated groups using the one-way analysis of variance, followed by Bonferroni's *post hoc* test using GraphPad Prism™ (version 6.0; GraphPad Software, (California, USA)). For body weight comparison within the same group of animals at two different times (0 and 24 h after PAA-coated ION administration), the paired *t*-test was performed. $P < 0.05$ was considered statistically significant. Outliers were identified using the ROUT method ($Q = 1\%$).

Results

Plasma levels of creatine kinase increased, while aspartate aminotransferase and alanine aminotransferase were not altered after intravenous administration of polyacrylic acid-coated iron oxide nanoparticles

As presented in Table 1, no significant differences were found in plasma levels of AST or ALT from control mice (administered with 0.9% saline solution) and PAA-coated IONs treated mice (8, 20 or 50 mg kg^{-1}). Only the plasma levels of CK in the 8.0 mg kg^{-1} PAA-coated ION-treated group were found significantly increased, when compared to control animals. The 20 mg kg^{-1} dose group also showed a tendency to increased levels in plasma CK, although without reaching statistical significance (Table 1).

Number of large lymphocytes and neutrophils increased after administration of polyacrylic acid-coated iron oxide nanoparticles

Differential leukocyte counts performed in the blood of control mice and PAA-coated IONs treated mice (8, 20 or 50 mg kg^{-1}) showed: (1) an increase in the differential count of neutrophils after the two highest doses of PAA-coated IONs; (2) the differential count of small lymphocytes was lower in the 50 mg kg^{-1} group; and (3) the differential count of large lymphocytes increased (almost double in the 50 mg kg^{-1} group) when compared to the control group (Table 2). No significant differences were observed for monocytes, eosinophils or basophils between groups.

Administration of polyacrylic acid-coated iron oxide nanoparticles led to a significant iron accumulation in liver, spleen and lung

Animals were weighed before and 24 h after PAA-coated IONs administration. After killing the animals, all collected organs were weighed. As shown in Table 3, organ weights were not changed when compared to control animals.

To evaluate the biodistribution of PAA-coated IONs, iron levels were measured in the liver, spleen, kidneys, brain, heart, testes, lungs and tail of control mice and PAA-coated IONs treated mice (8, 20 or 50 mg kg^{-1}) (Fig. 1). In treated animals, PAA-coated IONs accumulated mainly in the liver and spleen at the two highest

Table 1. Plasma levels of AST, ALT and total CK in CD-1 mice exposed to polyacrylic acid-coated iron oxide nanoparticles (0, 8, 20 or 50 mg kg^{-1})

U L^{-1}	Groups (mg kg^{-1})			
	0	8	20	50
AST	66.8 ± 17.3	50.7 ± 8.1	45.8 ± 8.5	38.8 ± 3.5
ALT	32.4 ± 5.4	33.0 ± 3.5	22.8 ± 1.9	25.3 ± 2.2
CK	58.5 ± 6.3	124.3 ± 22.6*	88.0 ± 6.9	81.7 ± 13.2

ALT, alanine aminotransferase; AST, aspartate aminotransferase; CK, creatine kinase.
Values are presented as mean ± SEM, $n = 4–6$ per group. *$P < 0.05$ when compared to control (mice administered with 0.9% saline solution).

Table 2. Leukocyte differential counts for mice injected with polyacrylic acid-coated iron oxide nanoparticles (0, 8, 20 or 50 mg kg^{-1})

Leukocytes (%)	Groups (mg kg^{-1})			
	0	8	20	50
Neutrophils	12.0 ± 0.6	15.8 ± 0.8	18.7 ± 0.8**	21.2 ± 2.0****
Small lymphocytes	75.5 ± 0.7	68.2 ± 2.4	68.8 ± 2.6	60.0 ± 2.5***
Large lymphocytes	8.5 ± 1.5	11.2 ± 2.6	10.2 ± 2.5	16.8 ± 1.4*
Monocytes	3.0 ± 1.0	4.3 ± 0.4	2.2 ± 0.7	2.0 ± 0.9
Eosinophils	0.3 ± 0.2	0.0 ± 0.0	0.0 ± 0.0	0.0 ± 0.0
Basophils	0.7 ± 0.3	0.5 ± 0.3	0.2 ± 0.2	0.0 ± 0.0

Values are presented as mean ± SEM, $n = 6$ per group. ****$P < 0.0001$, ***$P < 0.001$, **$P < 0.01$ and *$P < 0.05$ when compared to control (mice administered with 0.9% saline solution).

Table 3. Body and organs weight of CD-1 mice administered with polyacrylic acid-coated iron oxide nanoparticles (0, 8, 20 or 50 mg kg^{-1})

Parameters	Groups (mg kg^{-1})			
	0	8	20	50
0 h, body weight (g)	34.50 ± 0.62	32.83 ± 0.40	33.33 ± 0.99	33.50 ± 1.18
24 h, body weight (g)	34.33 ± 0.61	32.75 ± 0.79	32.83 ± 1.11	33.00 ± 1.03
Liver weight/total weight ratio (%)	6.55 ± 0.29	6.65 ± 0.15	6.30 ± 0.15	6.46 ± 0.31
Spleen weight/total weight ratio (%)	0.38 ± 0.01	0.39 ± 0.02	0.39 ± 0.02	0.41 ± 0.04
Lungs weight/total weight ratio (%)	0.52 ± 0.02	0.51 ± 0.01	0.51 ± 0.02	0.51 ± 0.04
Kidneys weight/total weight ratio (%)	1.60 ± 0.92	1.77 ± 0.06	1.63 ± 0.08	1.81 ± 0.05
Brain weight/total weight ratio (%)	1.28 ± 0.06	1.27 ± 0.03	1.36 ± 0.05	1.47 ± 0.07
Heart weight/total weight ratio (%)	0.39 ± 0.01	0.38 ± 0.02	0.41 ± 0.01	0.40 ± 0.01
Testes weight/total weight ratio (%)	0.52 ± 0.01	0.59 ± 0.04	0.58 ± 0.03	0.62 ± 0.05

Values are presented as mean ± SEM, $n = 6$ per group.

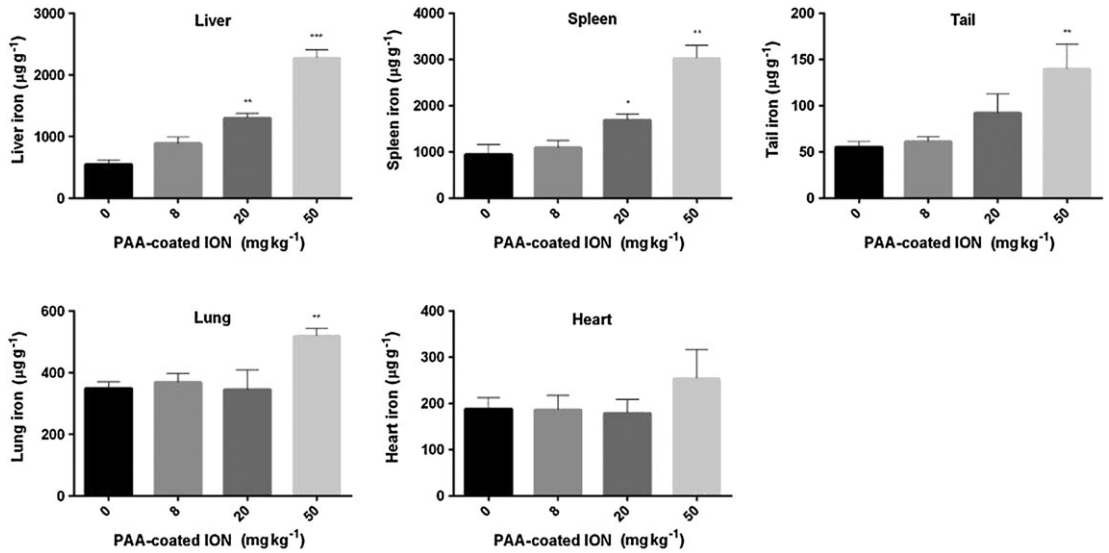

Figure 1. Iron biodistribution (liver, spleen, tail, lungs and heart) in CD-1 mice 24 h after i.v. administration of PAA-coated IONs (0, 8, 20 or 50 mg kg^{-1}). ***$P < 0.001$, **$P < 0.01$ and *$P < 0.05$ when compared to control (mice administered with 0.9% saline solution). Data are expressed as µg of iron g^{-1} of organ. Values are given as mean ± SEM ($n = 6$). ION, iron oxide nanoparticles; PAA, polyacrylic acid.

doses (20 and 50 mg kg^{-1}) and at the highest administered dose (50 mg kg^{-1}) in the lungs. One spleen sample showed no detectable level of iron, therefore, for statistical calculations, the missing value was imputed as limit of detection/√2, as previously described (Croghan and Egeghy, 2003). The calculated limit of detection for iron in the spleen was 614 µg g^{-1}.

Moreover, PAA-coated IONs showed a small tendency to accumulate in the heart (Fig. 1), although without statistical

significance. In contrast, the IONs did not accumulate in brain, kidneys or testes (data not shown). In the mice tail, iron levels increased in a dose-dependent manner, which suggests that some retention of PAA-coated IONs resulted from the i.v. administration.

Iron accumulates mostly in the periportal zone of the liver and in the red pulp of the spleen

Control animals showed normal liver histology. Iron-loaded Kupffer cells were found in dosed animals (Fig. 2A–D), whereas these were absent in control animals (Fig. 2E,F). Owing to the presence of iron, the cytoplasm of Kupffer cells was granular and golden brown on H&E staining (Fig. 2C). Exposed animals showed hepatic iron deposition, mostly in the periportal region but present in all hepatic acinus zones. The Perls' blue staining, confirmed this finding (Fig. 2B,D). In some liver areas, mainly in periportal regions, clusters of early necrotic hepatocytes were observed. These early necrotic cells showed increased cytoplasmic eosinophilia (Fig. 3). All the changes observed, were present in the entire organ. No hepatic collagen deposition, a marker of fibrosis and evidenced by Masson's trichrome staining, was detected.

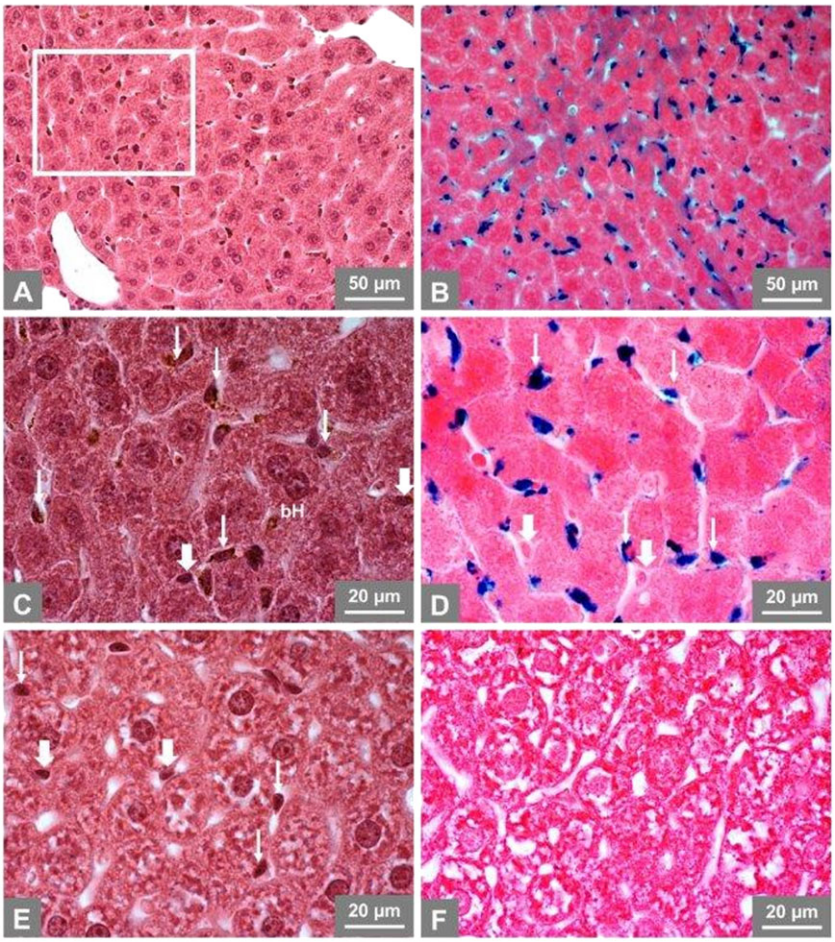

Figure 2. Light micrographs of paraffin sections from mouse liver stained with hematoxylin–eosin (A,C,E) and Perls' Prussian blue (B,D,F). Boxed area in (A) is shown at higher magnification in (C), where it is possible to observe that, with this staining, the Kupffer cell cytoplasm has a granular and golden brown appearance. bH, binucleate hepatocytes; thick arrows, endothelial cells; thin arrows, iron-loaded Kupffer cells.

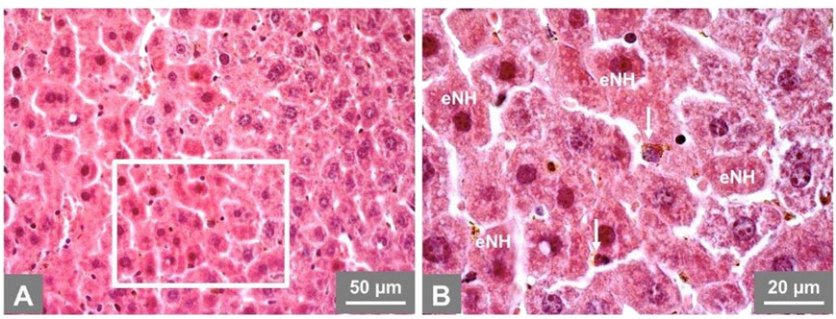

Figure 3. Light micrographs of paraffin sections from liver of mice exposed to polyacrylic acid-coated iron oxide nanoparticles (50 mg kg^{-1}) stained with hematoxylin–eosin. Boxed area is shown at higher magnification on the right (B). eNH, clusters the early necrotic hepatocytes; thin arrows, iron-loaded Kupffer cells.

Control animals exhibited normal spleen morphology on microscopic examination. Under light microscopy, no apparent alterations were observed in treated animals (at 50 mg kg^{-1}) on both H&E and Masson's trichrome stainings (Fig. 4A–C). No iron was detected by Perls' blue staining in the white pulp of both control and treated animals (Fig. 4D). When compared with the control mice (Fig. 4E), an increase in iron content was observed in splenic red pulp macrophages of treated animals (Fig. 4F) across the entire organ.

Histological examination of kidney sections from control and the 50 mg kg^{-1} group revealed a normal kidney organizational architecture. The renal corpuscles, proximal, distal and collecting tubules were found normal in treated animals (Fig. 5). No morphological alterations compatible with any sort of kidney pathology were observed (Fig. 5). No changes in iron distribution were observed in this organ in the two animal groups by the Perls' blue staining (data not shown).

Polyacrylic acid-coated iron oxide nanoparticles did not cause any significant change in liver or kidney glutathione

GSSG and GSHt levels were determined in the liver and kidney of all animals. Additionally, GSH and GSH/GSSG ratio were calculated.

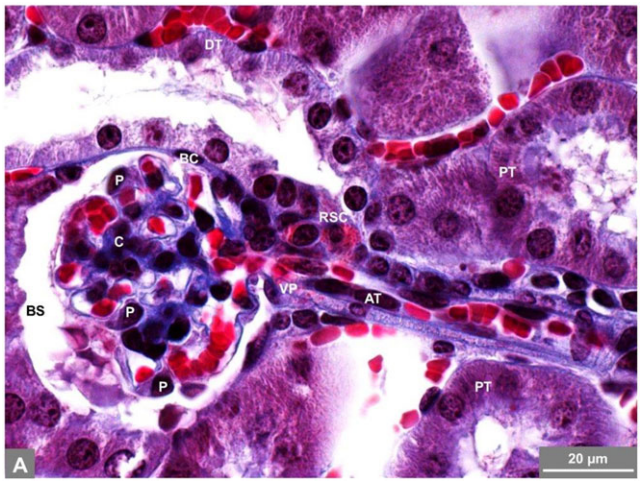

Figure 5. No histopathologic alterations were found in mice kidney after the treatment with polyacrylic acid-coated iron oxide nanoparticles (50 mg kg^{-1}). AT, afferent arteriole; BC, Bowman's capsule; BS, Bowman's space; C, renal corpuscle; P, podocytes; PT, proximal tubule; RSC, renin-secreting cell; VP, vascular polar. Masson's trichrome staining.

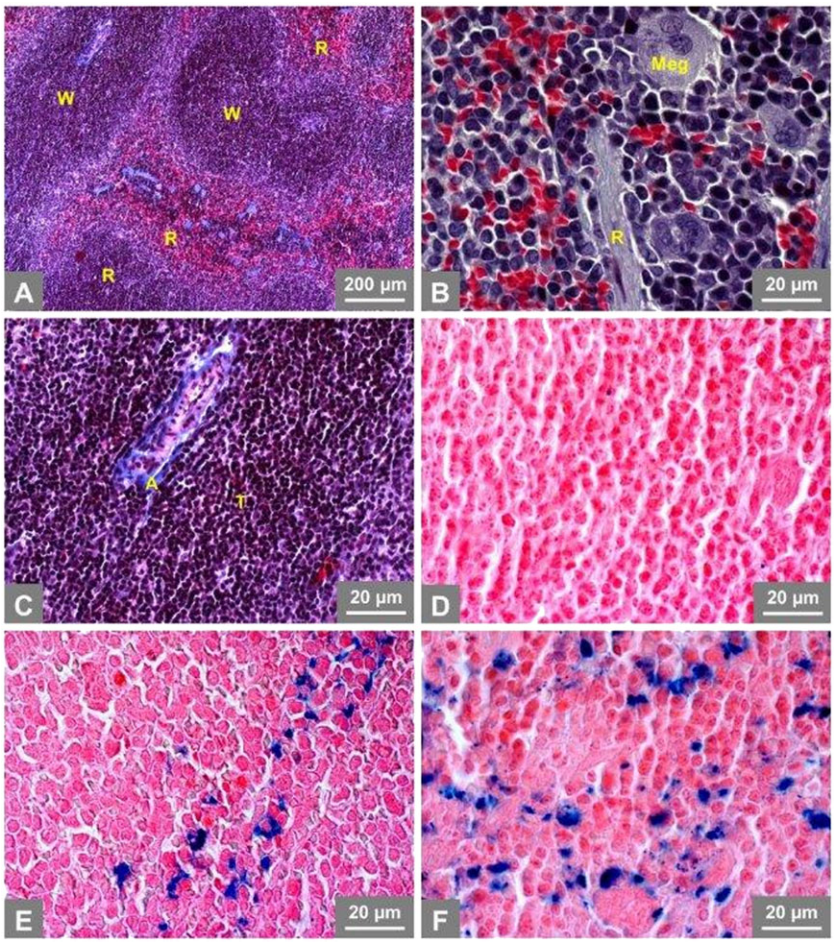

Figure 4. With Masson's trichrome staining (A–C) both control and polyacrylic acid-coated iron oxide nanoparticles (50 mg kg^{-1}) mice spleens showed a normal morphology (A), with a smaller proportion of red pulp. In mice, the splenic red pulp (B) is a major site of myeloid, erythroid hyperplasia and megakaryocytic hyperplasia. As shown in (C), the white pulp is a lymphoid area consisting of sheaths of lymphoid cells composed primarily of T cells around the central arteriole. No iron was detected in white pulp with the Perls' blue staining, in both the control and treated (D). When compared with the control (E), the splenic red pulp had a great amount of iron-laden macrophages in treated animals (F). A, arteriole; Meg, megakaryocyte; R, red pulp; T, T cells; W, white pulp.

It was observed that PAA-coated IONs did not alter GSSG, GSH and GSHt levels nor GSH/GSSH ratio in the mice's liver or kidney, even at the highest dose tested (50 mg kg^{-1}) (Table 4).

Polyacrylic acid-coated iron oxide nanoparticles caused hepatic lipid peroxidation at the highest dose tested

MDA levels were measured in the liver and kidney of control mice and mice previously administered with PAA-coated IONs (8, 20 or 50 mg kg^{-1}). It was clearly observed that PAA-coated IONs increased hepatic lipid peroxidation at the highest dose tested (50 mg kg^{-1}) when compared to control values. On the other hand, PAA-coated IONs did not exert any significant effect in the kidneys of mice regarding lipid peroxidation (Fig. 6).

Polyacrylic acid-coated iron oxide nanoparticles did not affect hepatic or renal adenosine triphosphate levels

ATP determination was performed in the liver and kidney of all groups tested. Some tendency to a decrease in ATP levels in mice liver at the highest PAA-coated IONs dose tested (50 mg kg^{-1}) was observed, but no statistical significance was reached (Table 4). In the kidney, PAA-coated IONs did not alter ATP levels when compared to control animals (Table 4).

Discussion

This work was undertaken to assess the biodistribution of PAA-coated IONs in different organs of CD-1 mice (liver, spleen, kidneys, brain, heart, testes and lungs) and the potential proinflammatory and toxic effects after a single i.v. administration with a time-point of 24 h. As major findings, it was observed that: (1) PAA-coated IONs accumulated in the liver, spleen and lungs; (2) PAA-coated ION-treated animals showed significant iron accumulation in macrophages mostly in the periportal zone of the hepatic acinus and in the splenic red pulp; (3) no significant blood cytokine activation occurred, although PAA-coated IONs caused significant changes both in the levels of neutrophils and in the activated lymphocytes; (4) PAA-coated IONs caused hepatic lipid peroxidation that was accompanied by early necrosis; (5) liver and kidney levels of GSH and ATP were not affected by PAA-coated IONs.

AST and ALT are parenchymal intracellular enzymes released into the systemic circulation when there is hepatocellular or cardiac injury, usually involving necrosis (Huang *et al.,* 2006). No significant differences were found in plasma levels of the AST or ALT in both control and PAA-coated IONs treated mice, thus suggesting that these NPs did not cause any substantial liver or heart necrotic damage. However, the histological examination of the animals treated with the highest IONs dose (50 mg kg^{-1}) showed foci of early necrotic cells. Whether the small number of cells was not enough to induce a significant change of aminotransferase plasma levels or if the cells have not yet released their content, are two possible hypotheses. On the other hand, the plasma CK levels of the group treated with 8.0 mg kg^{-1} PAA-coated IONs increased significantly when compared to control values. CK constitutes a marker of muscle damage (Marunak *et al.,* 2007). However, the 20 and 50 mg kg^{-1} PAA-coated IONs treated groups also showed a tendency to higher CK levels without reaching statistical signifi-

Table 4. GSHt, GSSG, GSH, ATP levels and GSH/GSSG ratio of CD-1 mice exposed to polyacrylic acid-coated iron oxide nanoparticles (0, 8 or 50 mg kg^{-1})

Parameters (nmol mg^{-1} protein)	Groups							
	Liver (mg kg^{-1})				Kidneys (mg kg^{-1})			
	0	8	20	50	0	8	20	50
GSHt	44.06 ± 4.60	46.18 ± 4.73	46.92 ± 3.90	48.19 ± 3.81	7.18 ± 1.98	7.30 ± 1.99	7.55 ± 1.73	7.78 ± 1.51
GSSG	1.16 ± 0.09	1.20 ± 0.08	1.34 ± 0.10	1.32 ± 0.14	0.12 ± 0.04	0.11 ± 0.02	0.11 ± 0.02	0.12 ± 0.02
GSH	41.74 ± 4.42	43.79 ± 4.60	44.24 ± 3.78	45.54 ± 3.58	6.93 ± 1.92	7.08 ± 1.95	7.33 ± 1.69	7.54 ± 1.47
GSH/GSSG ratio	35.54 ± 1.37	36.49 ± 2.57	33.32 ± 2.56	35.04 ± 2.03	54.11 ± 9.41	56.47 ± 8.70	65.26 ± 5.19	62.86 ± 8.05
ATP	7.92 ± 1.12	6.90 ± 1.02	7.22 ± 1.01	5.38 ± 0.70	1.43 ± 0.39	1.42 ± 0.38	1.22 ± 0.19	1.64 ± 0.18

ATP, adenosine triphosphate; GSH, glutathione; GSHt, total glutathione; GSSG, oxidized glutathione.
Values are presented as mean ± SEM, n = 6 per group.

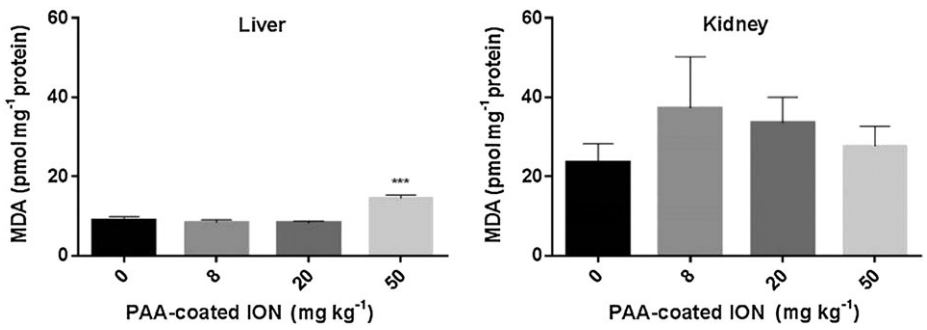

Figure 6. Hepatic and renal MDA evaluation in CD-1 mice 24 h after i.v. administration of PAA-coated IONs (0, 8, 20 or 50 mg kg^{-1}). ***$P < 0.001$ when compared to control (mice administered with 0.9% saline solution). Data are expressed as pmol MDA mg^{-1} protein. Values are given as mean ± SEM ($n \geq 5$). IONs, iron oxide nanoparticles; MDA, malondialdehyde; PAA, polyacrylic acid.

cance. In fact, changes in the values of serum CK after muscular damage follow a pattern, where there is a rapid release of CK after an injury and a fast plasma clearance, making plasma values return to basal normal values in mice in less than 24 h (Marunak *et al.,* 2007). Therefore, it is possible that, for the highest doses of administered iron, plasma CK values had already decreased to normal range or were decreasing to normal values at 24 h post-dosing with PAA-coated IONs. Nevertheless, the mechanisms behind the CK changes caused by PAA-coated IONs are yet to be elucidated.

Given that some IONs are reported to act on defense cells and inflammatory pathways (Couto *et al.,* 2014, 2015; Zhu *et al.,* 2011), these aspects were also addressed in the present study. An increase in the percentage of neutrophils, as well as in large lymphocytes, occurred for the highest dose tested of PAA-coated IONs (50 mg kg^{-1}). As neutrophils are the first line of innate host defense against pathogens and are associated with acute inflammations (Freitas *et al.,* 2008) and that small lymphocytes, when activated, transform into large lymphocytes (Portnoi *et al.,* 1986), the increased number of these cells may indicate an inflammatory process elicited by PAA-coated IONs. During the inflammatory cascade, several mediators may be produced and cytokines may exert pivotal roles in those processes. As lymphocytes, as well as neutrophils, are widely described as being cytokine producers, the potential effect of PAA-coated IONs in several plasma cytokine levels, such as IL-6, IL-10, IFN-γ, TNF-α and IL-12p70 and the chemokine monocyte chemoattractant protein-1, was evaluated. Despite the IONs induced increase in large lymphocytes and neutrophils at the highest tested dose, there were no changes elicited in plasma levels of cytokines/chemokine. We have recently shown, *in vitro*, that PAA-coated IONs (4 μg ml^{-1}) were able to activate extensively the production of several cytokines in human blood after a 24 h incubation period (Couto *et al.,* 2015). *In vivo*, cytokines have a rapid turnover and elimination; therefore, the half-life of most cytokines is usually minutes *in vivo*. *In vitro*, however, as there is a lack of renal and hepatic clearance, and therefore their half-life is substantially longer (Remick, 2003). We also hypothesize that, although rapid cytokine turnover can occur *in vivo*, the pharmacokinetic features of NPs may need a longer plasma exposure when compared to the *in vitro* studies. Induced cytokine production perhaps needs more time and, therefore, lymphocyte activation had not yet been reflected in the increase of cytokine levels. Chen and colleagues (2010) reported that 72 h after acute administration of non-coated IONs to ICR mice (0–51.4 mg kg^{-1}), the levels of IFN-γ, IL-2 and IL-10 were increased. Although one could advocate for coating differences regarding the previously mentioned study, in our previous *in vitro* study, we demonstrated that the extensive activation of the cytokines was independent of coating (Couto *et al.,* 2015). Therefore, exposure time seemed to be important for potential cytokine production *in vivo*. To verify the reliability of our methodologies, lipopolysaccharide was administered at different doses (5 and 15 mg kg^{-1} intraperitoneal [i.p.] injection) and exposure times (2 or 4 h) to CD-1 mice. The blood collected was used as a positive control and the administered lipopolysaccharide caused an increase in cytokines and the chemokine production (unpublished results).

The biodistribution of PAA-coated IONs, across the different organs was also studied herein. IONs mainly accumulated in liver, spleen and lungs. Iron is largely stored in ferritin, particularly in the cells of the liver, spleen and bone marrow, the former organs being involved in iron recycling from aged red cells through macrophages phagocytosis (Linder, 2013). Herein, PAA-coated IONs were taken up by macrophages in the liver (Kupffer cells) and spleen, confirming that these IONs have a specific uptake by the monocyte–macrophage system (Corot *et al.,* 2006). Histology of liver slices (Perls' staining) confirmed the presence of Prussian blue-positive stained cells mainly those in close contact with the main hepatic portal branches. IONs were also removed from the circulation by macrophages found in the red pulp of the spleen. A similar pattern of accumulation was also observed in a previous work (Yang *et al.,* 2015), where IONs coated with amphiphilic polymers containing carboxylic acid (total of 20 mg kg^{-1} in two i.v. injections 24 h apart) mainly accumulated in the liver and spleen of Kunming mice, followed by lungs and kidneys (Yang *et al.,* 2015). All organs contain iron, but the most highly ferruginous organs are liver and spleen, with the lungs also containing considerable amounts. In ICR mice given 600 mg kg^{-1} magnetic IONs by intragastric administration, the iron lung levels peaked at 6 h and then steadily decreased (Wang *et al.,* 2010). In the present study, we have observed that, for the highest dose of PAA-coated IONs tested (50 mg kg^{-1}), an iron accumulation in the lungs occurred. As the lungs have a very rich resident macrophage population that is reported to be able to phagocyte particles from the circulating blood (Brain, 1992), we believe that these macrophages were able to ingest the circulating PAA-coated IONs, as happens for the liver and spleen cells.

No significant differences were observed in iron content in the kidneys of controls and PAA-coated IONs treated animals. In the work of Wang *et al.* (2010), the iron content in the kidneys of magnetic IONs treated mice remained slightly above baseline during the whole observation period (up to 10 days after administration), indicating that renal excretion of iron is modest. Also in the present study, we have shown that PAA-coated IONs do not significantly cross the blood–brain barrier, while others have observed that albumin-coated γ-Fe_2O_3 (approximately 25 mg kg^{-1}, i.p. administration) were able to cross the blood–brain barrier in Swiss mice, reaching a maximum iron concentration at 48 h post-dosing (Estevanato *et al.,* 2011). In the study by Wang *et al.* (2010), magnetic IONs crossed the blood–brain barrier, although the underlying mechanisms were not determined. It seems that the sort of coating can have a determinant role in IONs distribution in these animal models.

Metal-containing NPs raise toxicity concerns because they can be quickly cleared from the blood by the reticuloendothelial system and can remain in organs such as the liver and spleen for prolonged periods (Almeida *et al.,* 2011; Wang *et al.,* 2010). Moreover, when a foreign body is internalized by phagocytes, an inflammatory process is triggered and production of inflammatory mediators and ROS may occur (Freitas *et al.,* 2009). We have demonstrated *in vitro* that these PAA-coated IONs induce ROS production (Couto *et al.,* 2014). It is also known that oxidative stress is involved in hepatic and renal damage elicited by IONs *in vivo* (Ma *et al.,* 2012). In this study, MDA levels increased in mice liver after treatment with the highest dose tested (50 mg kg^{-1}) when compared with control animals. To the best of our knowledge, this is the first time that PAA-coated IONs are reported to trigger MDA production *in vivo*. We hypothesize that this ROS generation occurred due to PAA-coated IONs internalization by liver phagocytes, which results in their activation and subsequent production of reactive species. The results obtained by Ma *et al.* (2012) also showed that IONs induced an increase of MDA in mice liver (20 mg kg^{-1} i.p., once daily, for a week). The hypothesis that the observed hepatic lipid peroxidation in the present work can lead to the necrotic foci observed at the highest dose tested needs further investigation. However, those necrotic foci were not sufficient to

cause a significant ALT and/or AST plasma increase or changes in ATP levels in comparison to control animals.

No significant differences were observed regarding hepatic GSH or GSSG levels. Ma and co-workers (2012) observed a significant decrease in GSH in Kunming mice liver and kidney after daily 40 mg kg^{-1} i.p. administrations of IONs for a week. The higher cumulative dose certainly affected the cytosolic redox status of these animals. Herein, no lipid peroxidation or GSH status alteration occurred in the kidney possibly because our PAA-coated IONs had no significant renal accumulation.

The obtained results in this pre-clinical study with PAA-coated IONs showed that they accumulate mainly in the liver and spleen and, to a lesser extent, in the lungs. Although our data showed that PAA-coated IONs do not cause severe organ damage, an inflammatory process seems to be triggered *in vivo*, as evidenced by the increased differential count of neutrophils and large lymphocytes in blood. Moreover, an accumulation of PAA-coated IONs in liver phagocytes was observed and hepatic lipid peroxidation was elicited showing that these NPs are able to induce oxidative stress. These effects need to be further investigated regarding the mechanisms involved as well as the consequences of long-term exposure to PAA-coated IONs.

Acknowledgments

We would like to thank FCT (Fundação para a Ciência e Tecnologia, Portugal) for the financial support to UCIBIO-REQUIMTE through the project UID/Multi/04378/2013. DC, MF and VMC acknowledge FCT financial support for the PhD and Post-doc grants (SFRH/BD/72856/2010, SFRH/BPD/76909/2011 and SFRH/BPD/63746/2009, respectively), within "POPH – QREN – Tipologia 4.1 – Formação Avançada" co-sponsored by FSE and national funds of MCTES. We greatly acknowledge Dr[a]. Laura Pereira for her assistance in the plasma determinations and Celeste Resende for her assistance in the histological procedures. We also acknowledge Professor José Alberto Duarte for allowing the use of his lab installations and the veterinarians in the ICBAS for their assistance with the animals.

Conflict of interest

The authors did not report any conflict of interest.

References

Ahamed M, Alhadlaq HA, Alam J, Khan MA, Ali D, Alarafi S. 2013. Iron oxide nanoparticle-induced oxidative stress and genotoxicity in human skin epithelial and lung epithelial cell lines. *Curr. Pharm. Des.* **19**: 6681–6690.

Alkins R, Burgess A, Ganguly M, Francia G, Kerbel R, Wels WS, Hynynen K. 2013. Focused ultrasound delivers targeted immune cells to metastatic brain tumors. *Cancer Res.* **73**: 1892–1899.

Almeida JP, Chen AL, Foster A, Drezek R. 2011. *In vivo* biodistribution of nanoparticles. *Nanomedicine* **6**: 815–835.

Anzai Y, Piccoli CW, Outwater EK, Stanford W, Bluemke DA, Nurenberg P, Saini S, Maravilla KR, Feldman DE, Schmiedl UP, Brunberg JA, Francis IR, Harms SE, Som PM, Tempany CM. 2003. Evaluation of neck and body metastases to nodes with ferumoxtran 10-enhanced mr imaging: Phase III safety and efficacy study. *Radiology* **228**: 777–788.

Bancroft JD, Gamble M. 2008. *Theory and Practice of Histological Techniques*. Churchill Livingston: London.

Bolliger AP, Everds NE. 2010. Hematology of laboratory rodents: mouse (*Mus musculus*) and rat (*Rattus norvegicus*). In *Schalm's Veterinary Hematology*, Weiss DJ, Wardrop KJ (eds). Wiley-Blackwell: Iowa, USA; 852–862.

Brain JD. 1992. Mechanisms, measurement, and significance of lung macrophage function. *Environ. Health Perspect.* **97**: 5–10.

Cao B, Qiu P, Mao C. 2013. Mesoporous iron oxide nanoparticles prepared by polyacrylic acid etching and their application in gene delivery to mesenchymal stem cells. *Microsc. Res. Tech.* **76**: 936–941.

Chen B-A, Jin N, Wang J, Ding J, Gao C, Cheng J, Xia G, Gao F, Zhou Y, Chen Y, Zhou G, Li X, Zhang Y, Tang M, Wang X. 2010. The effect of magnetic nanoparticles of Fe_3O_4 on immune function in normal ICR mice. *Int. J. Nanomed.* **5**: 593–599.

Corot C, Robert P, Idee JM, Port M. 2006. Recent advances in iron oxide nanocrystal technology for medical imaging. *Adv. Drug Deliv. Rev.* **58**: 1471–1504.

Couto D, Freitas M, Vilas-Boas V, Dias I, Porto G, Lopez-Quintela MA, Rivas J, Freitas P, Carvalho F, Fernandes E. 2014. Interaction of polyacrylic acid coated and non-coated iron oxide nanoparticles with human neutrophils. *Toxicol. Lett.* **225**: 57–65.

Couto D, Freitas M, Porto G, Lopez-Quintela MA, Rivas J, Freitas P, Carvalho F, Fernandes E. 2015. Polyacrylic acid-coated and non-coated iron oxide nanoparticles induce cytokine activation in human blood cells through TAK1, p38 MAPK and JNK pro-inflammatory pathways. *Arch. Toxicol.* **89**: 1759–1769.

Croghan C, Egeghy PP. 2003. Methods of dealing with values below the limit of detection using SAS. Presented at Southern SAS User Group, St. Petersburg, FL, September 22–24, 2003.

Dores-Sousa JL, Duarte JA, Seabra V, Bastos ML, Carvalho F, Costa VM. 2015. The age factor for mitoxantrone's cardiotoxicity: Multiple doses render the adult mouse heart more susceptible to injury. *Toxicology* **329**: 106–119.

Estevanato L, Cintra D, Baldini N, Portilho F, Barbosa L, Martins O, Lacava B, Miranda-Vilela AL, Tedesco AC, Bao S, Morais PC, Lacava ZG. 2011. Preliminary biocompatibility investigation of magnetic albumin nanosphere designed as a potential versatile drug delivery system. *Int. J. Nanomed.* **6**: 1709–1717.

Farrell BT, Hamilton BE, Dosa E, Rimely E, Nasseri M, Gahramanov S, Lacy CA, Frenkel EP, Doolittle ND, Jacobs PM, Neuwelt EA. 2013. Using iron oxide nanoparticles to diagnose CNS inflammatory diseases and PCNSL. *Neurology* **81**: 256–263.

Freitas M, Porto G, Lima JL, Fernandes E. 2008. Isolation and activation of human neutrophils *in vitro*. The importance of the anticoagulant used during blood collection. *Clin. Biochem.* **41**: 570–575.

Freitas M, Lima JL, Fernandes E. 2009. Optical probes for detection and quantification of neutrophils' oxidative burst. A review. *Anal. Chim. Acta* **649**: 8–23.

Hayes AW (eds). 2001. *Principles and Methods of Toxicology*, 4th edn. CRC Press.

Huang XJ, Choi YK, Im HS, Yarimaga O, Yoon E, Kim HS. 2006. Aspartate aminotransferase (AST/GOT) and alanine aminotransferase (ALT/GPT) detection techniques. *Sensors-Basel* **6**: 756–782.

Hudgins PA, Anzai Y, Morris MR, Lucas MA. 2002. Ferumoxtran-10, a superparamagnetic iron oxide as a magnetic resonance enhancement agent for imaging lymph nodes: A phase 2 dose study. *AJNR Am. J. Neuroradiol.* **23**: 649–656.

Iversen NK, Frische S, Thomsen K, Laustsen C, Pedersen M, Hansen PB, Bie P, Fresnais J, Berret JF, Baatrup E, Wang T. 2013. Superparamagnetic iron oxide polyacrylic acid coated γ-Fe_2O_3 nanoparticles do not affect kidney function but cause acute effect on the cardiovascular function in healthy mice. *Toxciol. Appl. Pharmacol.* **266**: 276–288.

Keller TM, Michel SC, Frohlich J, Fink D, Caduff R, Marincek B, Kubik-Huch RA. 2004. USPIO-enhanced MRI for preoperative staging of gynecological pelvic tumors: preliminary results. *Eur. Radiol.* **14**: 937–944.

Kooi ME, Cappendijk VC, Cleutjens KB, Kessels AG, Kitslaar PJ, Borgers M, Frederik PM, Daemen MJ, van Engelshoven JM. 2003. Accumulation of ultrasmall superparamagnetic particles of iron oxide in human atherosclerotic plaques can be detected by *in vivo* magnetic resonance imaging. *Circulation* **107**: 2453–2458.

Linder MC. 2013. Mobilization of stored iron in mammals: A review. *Nutrients* **5**: 4022–4050.

Ma P, Luo Q, Chen J, Gan Y, Du J, Ding S, Xi Z, Yang X. 2012. Intraperitoneal injection of magnetic Fe_3O_4-nanoparticle induces hepatic and renal tissue injury via oxidative stress in mice. *Int. J. Nanomed.* **7**: 4809–4818.

Mack MG, Balzer JO, Straub R, Eichler K, Vogl TJ. 2002. Superparamagnetic iron oxide-enhanced MR imaging of head and neck lymph nodes. *Radiology* **222**: 239–244.

Maier-Hauff K, Rothe R, Scholz R, Gneveckow U, Wust P, Thiesen B, Feussner A, von Deimling A, Waldoefner N, Felix R, Jordan A. 2007. Intracranial thermotherapy using magnetic nanoparticles combined with external beam radiotherapy: Results of a feasibility study on patients with glioblastoma multiforme. *J. Neurooncol* **81**: 53–60.

Maier-Hauff K, Ulrich F, Nestler D, Niehoff H, Wust P, Thiesen B, Orawa H, Budach V, Jordan A. 2011. Efficacy and safety of intratumoral

thermotherapy using magnetic iron-oxide nanoparticles combined with external beam radiotherapy on patients with recurrent glioblastoma multiforme. *J. Neurooncol* **103**: 317–324.

Marunak SL, Leiva L, Denegri MEG, Teibler P, de Perez OA. 2007. Isolation and biological characterization of a basic phospholipase A_2 from *Bothrops jararacussu* snake venom. *Biocell* **31**: 355–364.

McCauley TR, Rifkin MD, Ledet CA. 2002. Pelvic lymph node visualization with MR imaging using local administration of ultra-small superparamagnetic iron oxide contrast. *J. Magn. Reson. Imaging* **15**: 492–497.

Portnoi D, Freitas A, Holmberg D, Bandeira A, Coutinho A. 1986. Immunocompetent autoreactive lymphocytes B are activated cycling cells in normal mice. *J. Exp. Med.* **164**: 25–35.

Qiu D, Zaharchuk G, Christen T, Ni WW, Moseley ME. 2012. Contrast-enhanced functional blood volume imaging (CE-fBVI): Enhanced sensitivity for brain activation in humans using the ultrasmall superparamagnetic iron oxide agent ferumoxytol. *Neuroimage* **62**: 1726–1731.

Ramos P, Santos A, Pinto NR, Mendes R, Magalhaes T, Almeida A. 2014. Iron levels in the human brain: A post-mortem study of anatomical region differences and age-related changes. *J. Trace Elem. Med. Biol.* **28**: 13–17.

Remick DG. 2003. Cytokines and cytokine receptors: principles of action. In *Cytokines and Mental Health*, Kronfol Z (ed.). Kluwer Academic Publishers; Boston; 8–9.

Ross RW, Zietman AL, Xie W, Coen JJ, Dahl DM, Shipley WU, Kaufman DS, Islam T, Guimaraes AR, Weissleder R, Harisinghani M. 2009. Lymphotropic nanoparticle-enhanced magnetic resonance imaging (LNMRI) identifies occult lymph node metastases in prostate cancer patients prior to salvage radiation therapy. *Clin. Imaging* **33**: 301–305.

Rossato LG, Costa VM, Dallegrave E, Arbo M, Dinis-Oliveira RJ, Santos-Silva A, Duarte JA, Bastos MD, Palmeira C, Remiao F. 2014. Cumulative mitoxantrone-induced haematological and hepatic adverse effects in a subchronic *in vivo* study. *Basic Clin. Pharmacol. Toxicol.* **114**: 254–262.

Shubayev VI, Pisanic TR, 2nd, Jin S. 2009. Magnetic nanoparticles for theragnostics. *Adv. Drug Deliv. Rev.* **61**: 467–477.

Wang J, Chen Y, Chen B, Ding J, Xia G, Gao C, Cheng J, Jin N, Zhou Y, Li X, Tang M, Wang XM. 2010. Pharmacokinetic parameters and tissue distribution of magnetic Fe_3O_4 nanoparticles in mice. *Int. J. Nanomedicine* **5**: 861–866.

Weinstein JS, Varallyay CG, Dosa E, Gahramanov S, Hamilton B, Rooney WD, Muldoon LL, Neuwelt EA. 2010. Superparamagnetic iron oxide nanoparticles: diagnostic magnetic resonance imaging and potential therapeutic applications in neurooncology and central nervous system inflammatory pathologies, a review. *J. Cereb. Blood Flow Metab.* **30**: 15–35.

Yang L, Kuang H, Zhang W, Aguilar ZP, Xiong Y, Lai W, Xu H, Wei H. 2015. Size dependent biodistribution and toxicokinetics of iron oxide magnetic nanoparticles in mice. *Nanoscale* **7**: 625–636.

Zhu MT, Wang B, Wang Y, Yuan L, Wang HJ, Wang M, Ouyang H, Chai ZF, Feng WY, Zhao YL. 2011. Endothelial dysfunction and inflammation induced by iron oxide nanoparticle exposure: risk factors for early atherosclerosis. *Toxicol. Lett.* **203**: 162–171.